RSC Advances

ROYAL SOCIETY OF CHEMISTRY

www.rsc.org/advances

Characterization and corrosion behavior of Co and Co–P coatings electrodeposited from chloride bath

V. Ezhilselvi, H. Seenivasan,[a] Parthasarathi Bera,[*] Chinnasamy Anandan

Surface Engineering Division, CSIR–National Aerospace Laboratories, Bangalore 560017, India

Abstract

Co–P coatings with low and high phosphorous contents are electrodeposited using direct current (DC) and pulse current (PC) methods from cobalt chloride baths. Low phosphorous content coatings obtained from DC and PC methods are crystalline with predominantly fcc structure while the high P content coatings are amorphous. Electrochemical corrosion studies demonstrate an increase in corrosion resistance with increase in phosphorous in both DC and PC plated coatings. PC coatings show higher polarization resistance (R_p) and lower corrosion current density (i_{corr}) indicating better corrosion resistance of these coatings. Compositional analysis shows a slight or no increase in P content after corrosion in PC coatings with high P content exhibiting better corrosion resistance. Comparisons of surface morphologies before and after corrosion illustrate that PC plated coatings are less affected compared to their DC counterparts. Higher amount of oxidized cobalt in PC electrodeposited coatings is deduced from X-ray photoelectron spectroscopy (XPS) while mainly metallic Co species is found in DC plated coatings. This study demonstrates that the overall corrosion resistance for the PC deposited coatings is better than the DC deposited coatings owing to reasons like high P content, amorphous structure, smooth morphology and higher metal oxide content in the deposits.

---

*Corresponding author

Tel: +91–80–25086359, Fax: +91–80–25210113, E mail: partho@nal.res.in (P. Bera)

[a]Present address: Department of Chemical Sciences, Indian Institute of Science Education and Research Kolkata, Mohanpur 741252, West Bengal, India

1. Introduction

Usage of hard chromium as protective coating in several automobile and aerospace applications has nowadays become a greatest environmental issue due to the presence of carcinogenic chromium (VI) in the electrolplating bath. Recently, Co–P coatings have been identified as the suitable material for hard chromium replacement as they exhibit excellent mechanical wear and corrosion resistance and high thermal stability.[1–4] Their properties are mainly influenced by the amount of phosphorous present in the coatings which helps in the enhancement of properties by transforming cobalt alloys from crystalline to amorphous. Previous studies on Co–P alloys showed that alloys greater than 6 wt.% P exhibited amorphous structure.[5–8] Available literature on Co–P coatings reveal that high phosphorous content alloys can be achieved by PC plating compared to DC plating.[7–10] These coatings show improved properties in comparison with their DC plated counterparts. Increased P content is attributed to the migration of hypophosphite anions near the cathode during the off-time provided in the PC electrodepositon. Also, better corrosion resistance observed in amorphous alloy is due to the absence of grain boundaries and secondary phase particles which act as active sites for corrosive attack. Recent review on corrosion behavior of nanocrystalline materials emphasizes the role of coexisting alloying elements (metals or nonmetals) which usually enhance the corrosion resistance by acting synergistically with the base metal.[11]

Microstructure,[12,13] microhardness,[9] thermal stability[3,4] and magnetic properties[14,15] of Co–P alloys obtained from different plating conditions have been well studied. Though few reports are available on the wear[1,2] and corrosion behavior of Co–P coatings, in-depth understanding of these technologically important properties is not yet attained. Number of researchers have shown interest towards the corrosion behavior of Co–P alloys in acidic, alkaline

and neutral media.[7,16–21] Comparison of the electrochemical corrosion behavior of DC and PC plated low and high phosphorous content Co–P alloy coatings from sulfamate bath was studied by Ezhilselvi and coworkers.[7] Increase in P content increased the corrosion resistance and after a certain limit it had a detrimental effect on the coatings. Pulse plated Co–P alloys resisted corrosion better when compared to their DC plated counterparts. In the corrosion studies of Co–P and Ni–P coatings with high phosphorous content in oxygen atmosphere, Gillot et al. demonstrated that as-deposited alloys was oxidized to form an outer oxide layer while the inner layer was enriched by phosphorous.[16] At higher temperatures, phosphide crystals of Co and Ni make a continuous layer which resists further oxygen penetration. Jung and Alfantazi in two separate studies, examined the corrosion behavior of as-deposited and heat treated nanocrystalline Co and Co–P alloys (Co 1.1 wt.% P and Co 2.1 wt.% P) in 0.1M H_2SO_4 solution.[18,19] An enhanced corrosion resistance was observed by the authors when phosphorous was added into the coatings, whereas annealing the samples led to poor corrosion resistance due to the segregation of Co in the grain boundaries and the formation of Co_2P. EDX and XPS studies confirmed the P enrichment on the surfaces was due to the preferential dissolution of cobalt. A detailed study by Helfand et al. on the role of P in the anodic inhibition of amorphous Co–20P alloy in acidic electrolytes found that this coating showed a better corrosion resistance than pure Co. Their XPS studies showed enrichment of P in the form of hypophosphite and phosphate ions.[20]

In existing literature it has been demonstrated that the Co and Co–P coatings dissolve actively and they are not observed to passivate. The enrichment of the surface by P has also been shown to inhibit the corrosion to some extent. The present study is aimed at investigating the detailed corrosion behavior of Co–P coatings obtained from DC and PC electrodeposition

methods from chloride based baths. Composition, microstructure and morphology of as-deposited and corroded coatings have been characterized by EDXS, XRD and FESEM, respectively. For understanding of detailed electronic structure of these coatings XPS has also been carried out. XPS also helps in differentiating the nature of low and high P coatings and identifying the species present on the surface and their concentrations which leads to better understanding the corrosion mechanism of such technologically important coatings.

2. Experimental methods

2.1 Preparation

Cobalt coatings were electrodeposited from baths containing cobalt chloride (60 g L^{-1}) and phosphoric acid (20 ml L^{-1}) by DC and PC electrodeposition methods. Six (three DC and three PC) different Co–P alloy coatings with varying P content were obtained by adding 2, 5 and 10 g L^{-1} NaH_2PO_2 into the above prepared baths. The pH of prepared bath was around 1.8 and the pH was adjusted to 2.0 ± 0.05 by the addition of 10% NaOH. Temperature of the bath was maintained at 60 °C using a constant temperature water bath. Plain cobalt deposit was obtained from the same bath in the absence of hypophosphite. Analytical grade chemicals and deionized water were used to prepare the baths. For electrodeposition, approximately 200 mL solution was taken in a 250 mL glass beaker. Mild steel specimens of dimension 14.8 mm diameter and 6 mm thickness were degreased in acetone, cathodically cleaned in 10% NaOH solution for 2 min at 7 A dm^{-2}, rinsed in running water and then in deionized water. The degreased samples were deoxidized in 50% H_2SO_4 for 30 s, rinsed in running water and deionized water and then placed into the bath for electrodeposition. Direct current electrodeposition was carried out galvanostatically by using Aplab 7253 regulated DC power supply at average current density (i_{av}) of 7.7 A dm^{-2}. Pulse current electrodeposition was carried out galvanostatically using

cathodic square wave unipolar double pulse plating rectifier. The deposition was carried out at average current density (i_{av}) of 7.7 A dm^{-2} and the peak current density of 38 A dm^{-2}. The on-time (t_{on}) and off-time (t_{off}) were kept constant at the ratio of 1:4. Graphite bar contained in a pretreated anode bag was used as the anode. The thickness of coatings was maintained at 20 ± 2 μ. DC and PC plated samples are designated as DC Co, DC Co–P 1, DC Co–P 2, DC Co–P 3, PC Co, PC Co–P 1, PC Co–P 2 and PC Co–P 3 where 1, 2, 3 stand for baths containing 2, 5 and 10 g L^{-1} NaH_2PO_2, respectively.

2.2 Electrochemical corrosion

Potentiodynamic polarization and electrochemical impedance spectroscopy (EIS) experiments were performed using Autolab PGSTAT30 galvanostat/potentiostat instrument. The measurements were performed using a conventional three-electrode cell, in which test sample was placed in Teflon sample holder and the exposed surface area to the corrosive medium was approximately 0.785 cm^2. The platinum strip of 1 cm^2 area was served as counter electrode and Ag/AgCl, 3M KCl electrode was used as the reference electrode. Prior to the beginning of EIS measurements the sample was immersed in the corrosive medium (3.5% NaCl, pH6) for about 1 h in order to establish the open circuit potential (E_{OCP}) or the steady state potential. Both potentiodynamic polarization and electrochemical impedance spectroscopy experiments were performed in non-deaerated condition.

EIS measurements were conducted using a frequency response analyzer (FRA). The spectrum was recorded in the frequency range of 10 mHz–100 kHz with data density of 7 points per decade. The applied alternating potential had root mean square amplitude of 10 mV on the $E_{OCP.}$ After each experiment the impedance data was displayed as Nyquist and Bode plots. The Nyquist plot is a plot of real impedance (Z') versus imaginary impedance (Z''). At high

frequency the value of solution resistance (R_s) is obtained and at the low frequency the charge transfer resistance (R_{ct}) is deduced. The Bode plot is a plot of log|Z| versus log*f* and log*f* versus phase angle (θ) where |Z| and *f* are absolute impedance and frequency, respectively. A circuit description code (CDC) was assigned for the acquired data and the acquired data were curve fitted and analyzed using EQUIVCRT program.[22]

After EIS measurements, the system was allowed to attain its stable open circuit potential. After the stable open-circuit potential has been established the upper and the lower potential limits of linear sweep voltammetry was set ± 200 mV with respect to E_{OCP}, respectively. The sweep rate was 1 mV/s. The Tafel plot was obtained after the electrochemical measurements. The corrosion potential (E_{corr}), the corrosion current density (i_{corr}) and polarization resistance (R_P) values were deduced from Tafel plot (that is log*i* versus *E* plot). The corrosion current was obtained using Stern-Geary equation.[23]

2.3 Characterization

The structure of alloy deposits was determined by XRD studies employing a PANalytical X'Pert PRO X-Ray diffractometer operated with CuKα radiation of 1.5418 Å wavelength at 40 kV and 30 mA in the 2θ range 30−80°. The surface morphology and composition of as-deposited and after-corrosion alloy coatings were examined by FESEM using a Carl Zeiss Supra 40VP coupled with INCAPentaFETx3 energy dispersive X-ray spectrometer (EDXS) from Oxford Instruments. XPS of several as-deposited and after-corrosion Co–P alloy coatings were recorded with a Thermo Fisher Scientific Multilab 2000 spectrometer using non-monochromatic AlKα radiation (1486.6 eV) as an X-ray source operated at 150 W (15 kV and 10 mA). The binding energies reported here were calculated with reference to C1s peak at 284.5 eV with a precision of ± 0.1 eV. All the spectra were obtained with pass energy of 30 eV and step increment of 0.05 eV.

3. Results and discussion

3.1 XRD studies

Fig. 1 displays the XRD patterns of as-deposited Co–P deposits obtained by direct and pulse current methods. Plain Co and Co–P deposits with less than 4 wt.% P show crystalline behavior while the deposits with higher amount of phosphorous are amorphous. A high intensity peak at 75.4° observed for the plain Co coatings obtained from both DC and PC methods clearly corresponds to the (110) preferred orientation of fcc-cobalt. XRD pattern of DC Co–P 1 coating (3.7 wt.% P) contains two peaks at 41.2 and 46.9° corresponding to the (100) and (101) faces of hcp-cobalt. PC Co–P 1 coating obtained from similar bath (2.5 wt.% P) also shows two peaks at 41.2 and 47.0°. On contrary to PC Co–P 1 coating, an additional faint peak at 44.2° is observed in DC Co–P 1 coating which is due to (111) phase of fcc-Co. Appearance of this peak is attributed to the higher phosphorous content of the DC Co–P 1 coating in relation to PC Co–P 1 coating. In both the coatings, transformation from hcp-Co to fcc-Co occurs due to the inclusion of P into the lattice. Further increase in the phosphorous content is the reason for the amorphous nature of the coatings (DC and PC Co–P 2 and Co–P 3) formed from the baths containing 5 and 10 g L^{-1} NaH_2PO_2. Here, it is to be pointed out that the pH of the bath used in this study is acidic (pH2). Previous reports suggested that the Co coatings obtained at low pH values preferred fcc structure.[24,25] Therefore, formation of fcc-Co at such low pH value in the present study agrees well with the literature. Co deposits formed from the acidic solution were predominantly fcc, regardless of the deposition potential.[24] When the pH was raised to pH7, the fcc cobalt was transformed to hcp phase with a preferred orientation of (002) plane. However, deposition at higher voltage resulted in fcc plated cobalt with a preferred orientation of (111) planes. Nakahara and Mahajan showed by TEM analysis that low pH (~1.6) deposit from sulfate bath was highly

faulted fcc with some hcp regions.[25] At, pH~5.7 the density of the faults were greatly reduced and the structure was predominantly hcp. Several researchers reported that the pH of the bath solution significantly affected the structure of cobalt formed by electrodeposition.[26] A solution with low pH (<2.5) was reported to favor fcc cobalt, whereas a solution containing high pH (>2.5) or a bath with high temperature favored hcp cobalt. High deposition temperature in a chloride bath induced the formation of hcp cobalt,[27] whereas high current densities in sulfamate bath were found to favor the cubic structure.[28] The transition from β(fcc) to α(hcp)-Co was observed to occur in the pH range 2.5–3.0.[24] Earlier results put forward that increase in pH, temperature and current density led to the transformation from fcc- to hcp-cobalt. In this study, it has also been observed that in addition to the above said factors P inclusion also induces the structure change from fcc- to hcp-cobalt.

3.2 Corrosion studies

Potentiodynamic polarization curves of DC and PC plated Co and Co–P alloys in non-deaerated 3.5% NaCl solution are presented in Fig. 2. Behavior of mild steel (MS) substrate is also added for comparison. The corrosion parameters calculated for both the coatings using Tafel extrapolation method are given in Table 1. Cobalt coatings electrodeposited by both DC and PC techniques show a shift in corrosion potential to the positive side compared to that of uncoated MS substrates. Inclusion of P in the Co coatings significantly shifts the corrosion potential to the nobler side showing the efficiency of P containing coatings in protecting against corrosion attack. DC Co–P1 coating with 3.7 wt.% P shows a lower corrosion potential (E_{corr}) in relation to that of PC Co–P 1 with comparatively lower content of phosphorous (2.5 wt.% P). Though P content in DC plated coating is higher, corrosion resistance is lower in this case. This behavior is

due to the difference in surface morphology (see FESEM studies in later section) between these two coatings. Addition of P up to 8 wt.% in the case of DC and to 8.6 wt.% in the case of PC coating increases the corrosion resistance, while the resistance of the PC plated coating is higher. Further addition of hypophosphite up to 10 g L^{-1} NaH_2PO_2 increases the phosphorous content in the coating to 9.4 and 11.2 wt.% for DC Co–P 3 and PC Co–P 3 coatings, respectively. Corrosion potentials are –0.480 and –0.411 V for DC Co–P 3 and PC Co–P 3 coatings, respectively and show a shift in corrosion potential to nobler side. Corrosion current densities (i_{corr}) for DC Co–P3 and PC Co–P3 further decrease in relation to DC Co–P2 and PC Co–P2 but the i_{corr} and R_p values obtained for DC Co–P3 and PC Co–P3 coatings are comparable. This indicates improved resistance of the coatings and also shows that at higher P content DC and PC exhibit similar behavior. Increase in corrosion resistance with P content is also observed in previous studies.[7,19,21] Jung and Alfantazi also obtained an improved corrosion resistance of Co 2.1% P alloy when compared to the Co 1.1% P alloy.[19] A comparative study of the corrosion behavior of Co–P coatings with low and high phosphorous demonstrated that high P content coatings were amorphous and showed better corrosion resistance in relation to the coatings with low P concentration.[20] Present results are different from the previous works done by Ezhilselvi et al. on Co–P coatings obtained from sulfamate baths which showed lower corrosion resistance for very high phosphorous coatings (10 g L^{-1} NaH_2PO_2) from both DC and PC methods.[7] Difference observed in this study is due to the usage of chloride containing baths from which smooth coatings can be obtained even at high phosphorous content as discussed in FESEM section.

Figures 3 and 4 show Nyquist and Bode plots obtained for mild steel, plain Co and Co–P coatings prepared by DC and PC plating, respectively in 3.5% NaCl solution at their respective open circuit potentials in non-deaerated condition. In both cases, all the curves (Nyquist plots)

appear to be similar consisting of semicircle in the high frequency region signifying the charge controlled reaction. However, it is to be noted that though these curves appear to be similar with respect to their shape, they differ considerably in their diameter. Bode plots (log f versus log|Z| and log f versus θ) of Co–P coatings in Figs. 3 and 4 show a single peak inflection point in the plot of log f versus log|Z| and a single phase angle maximum in the plot of log f versus θ. A similar conclusion of the existence of a single capacitive loop has been reported by Jung and Alfantazi for the corrosion of nCo–1.1P and nCo–2.1P in 0.1M H_2SO_4 medium.[18] The single time constant can be attributed to the pore free dense uniform coating where whole surface is corroded in a similar fashion. In this study, the phase angle maximum varied from 70 to 80° for all coatings. For mild steel substrate the phase angle is around 60° indicating the inhomogenety of the surface due to its direct exposure to the aggressive medium. An equivalent electrical circuit model given in Fig. 5 has been utilized to simulate the electrode/solution interface and to analyze the acquired data. It consists of a double layer capacitance that is parallel to the charge transfer resistance, both of which are in series with the solution resistance between the working electrode (WE) and the tip of the Luggin capillary. This is the commonly proposed equivalent circuit model for the simple corrosion system which is entirely under charge transfer control. In this study, the coating and the substrate together have been represented as an electrode. The double layer capacitance provides information about the polarity and the amount of charge at the electrode/electrolyte interface. The capacitance is replaced with constant phase element (CPE) for a better quality fit. CPE amounts for the deviation from ideal dielectric behavior and is related to the surface inhomogeneities. It must be noted that in EQUIVCRT program, Q stands for constant phase element.[29,30] The CDC for the equivalent circuit proposed for mild steel substrate and the coatings is R(QR). The charge transfer resistance (R_{ct}) and the double layer

capacitance (Q_{dl}) obtained for DC and PC deposited Co–P alloy coatings are compiled in Table 2. R_{ct} values for DC deposited Co–P coatings vary from 5.0 to 13.6 kΩ cm^2. The high values of R_{ct} in the range of 23.8–45.8 kΩ cm^2 obtained for PC deposited Co–P coatings imply a better corrosion protective ability of these coatings. Among all the coatings, highest R_{ct} value is observed in PC Co–P 3 coating showing best corrosion resistance. Values of n_{dl} obtained for all these DC and PC coatings vary from 0.80 to 0.94. Q_{dl} values for DC coatings vary from 12.7 to 25.7 μSs^n cm^{-2}, whereas these values for PC coatings are 39.7 to 5.8 μSs^n cm^{-2}. Very low Q_{dl} value of PC Co–P 3 coating indicates compact and homogeneous morphology that results the better quality of the coating. From the above results, it can be understood that pulse deposited coatings exhibit higher corrosion resistance than DC deposited coatings. Higher n values for PC coatings indicate the homogeneous, smooth and pore-free deposits which can be attributed to single time constant behavior.

In the present study, Co–P coatings (both DC and PC) show crystalline behavior at low P content while at high phosphorous content they are amorphous according to XRD studies. Though these two types of coatings seem similar in their structure, morphological studies show that PC coatings are smooth and compact when compared to the DC plated ones (See FESEM section). This difference in morphology is the reason for increased corrosion resistance in the pulse plated coatings.

3.3 Chemical compositions

The chemical composition of as-deposited and corroded Co–P coatings were examined by EDXS and their values are given in the Table 3. DC Co–P coatings contain about 3.7–9.4 wt.% P whereas PC Co–P coatings show 2.5–11.2 wt.% P indicating that the pulse deposited coatings contain higher phosphorous content than DC deposited coatings. Similar results were reported

for Ni–P coatings in which pulse deposited coatings exhibited high phosphorous content than DC coatings.[31] EDX analysis has also been carried out on the corroded samples to find out the composition of corrosion products. Overall, there is a slight increase in P content after corrosion in all coatings except PC Co–P 3 (Table 3). But, a significant increase of P after corrosion in the coatings with low phosphorous such as DC Co–P 1 and PC Co–P 1 has been observed. This shows that cobalt in the low P content Co–P coatings dissolves during the corrosion process leading to lower corrosion resistance of these coatings. Slight increase of P content in the other coatings suggests dissolution of lesser amount of cobalt resulting in better corrosion resistance than the low P counterparts.

3.4 FESEM studies

The surface morphologies obtained from FESEM of the Co and Co–P alloys electrodeposited with DC and PC methods are shown in the Figs. 6 and 7, respectively. Fig 6 (a–d) shows morphology of DC deposited Co and Co–P 1, Co–P 2 and Co–P 3 coatings, respectively. Fig. 6(a) shows the surface morphology of plain cobalt with fibrous structure. When the phosphorous content increases, the fibrous structure transforms to larger distinct smooth dense nodules in nanosized grains. Further increase in P content results in larger nodular structure surrounded by smaller nodules indicating amorphous nature of the deposits (see XRD section). Fig. 7 (a–d) shows surface morphology of pulse deposited Co and Co–P 1, Co–P 2 and Co–P 3 coatings, respectively. Among the pulse deposited coatings, plain Co coating (Fig. 7a) exhibits randomly distributed fibrous structure which is typical characteristic of crystalline Co deposits, whereas Co–P coatings show smooth morphology with some nodules (Fig. 7 b–d). Phosphorous addition has played a major role in transforming the fibrous structure to fine grain structure. On

comparison, it has been found that, DC Co–P 1 exhibits spherical nodular morphology while the surface of PC Co–P 1 is relatively smooth. Rough surfaces are usually vulnerable to corrosion attack because of the heterogeneity and the possible presence of grain boundaries. On the other hand, smooth surfaces seem visually homogeneous, on which the feasibility of preferential attack is less. However, high P coatings (8–11 wt.%) in general are amorphous in nature and are evident from XRD studies. Morphologies of amorphous coatings appear to be smoother and brighter than the coatings having crystalline structure.[32] Sheikholeslam et al. reported the similar morphology for amorphous Co–P (9–11 wt.%) and they mentioned those nodules as "bumps".[13] They also observed that each bump in the nodular structure contained thousands of nanosized grains. Fig. 7 (d) shows the surface morphology of PC Co–P 3 which appears as the alternative ridges and the valleys with fine grains. Similar morphology was reported for cadmium deposits prepared at peak current density of 5000 A dm^{-2} and t_{off} of 100 ms[33] wherein fine structure can be due to blockage of the nucleation sites by the inhibitors (sulfate ions) during pulse off-time that facilitates the formation of new nuclei rather that depositing on the previous nuclei. In our study, the inhibitors are probably phosphate ions.

FESEM images of corroded surfaces of DC and PC deposited Co–P coatings are shown in Figs. 8 and 9, respectively. Fig. 8 (a–d) shows the corroded morphology of DC deposited coatings. Plain Co coating [Fig. 8 (a)] shows the irregular surface with acicular like structure. White colored regions are observed over the surface. Coarse nodular structure with fine fibrous structure is observed on the corroded surface of DC Co–P 1 coating [Fig. 8 (b)], whereas corroded surface of DC Co–P 2 coating [Fig. 8(c)] shows larger distinct coarse nodules with fine fibrous structure. Corroded surface of the coatings appears to be affected by the uniform corrosion over the surface. Fig. 8(d) corresponds to the corroded regions of DC Co–P 3 coating.

The morphologies of corroded surface of PC deposited coatings are also examined using FESEM and displayed in Fig. 9 (a–d). Fig. 9 (a) shows the corroded region of pulse deposited Co coating. Dark and bright regions appear over the surface. At higher magnification it is clearly seen that the characteristic fine grain ridged structures of PC deposited Co coating gets dissolved due to uniform corrosion nearly same as DC deposited Co coating. PC Co–P 1 [Fig. 9 (b)] shows the fine acicular structure over the surface due to uniform attack in the corrosive medium. In Fig. 9 (c), PC Co–P 2 exhibits smooth grayish surface with nodules. The P content has not changed significantly after corrosion. Fig. 9 (d) shows the corroded regions of PC Co–P 3 coating. No appreciable change in the morphology is observed in this coating after corrosion indicating the high quality of this coating that supports lowest Q_{dl} value obtained from its EIS data.

3.5 XPS studies

XPS was employed to get useful information on the elemental composition and their oxidation states in the surface of both as-deposited and corroded Co–P alloy coatings obtained from baths containing different NaH_2PO_2 concentrations. XPS of Co coatings are also carried out for comparison. In Fig. 10, XPS of Co2p core level spectra in as-deposited DC and PC Co and Co–P coatings and the same after corrosion are displayed. Co2p spectral envelops indicate that there are several Co2p component peaks in all these spectra and they are curve fitted into sets of spin-orbit doublets along with associated satellite (S) peaks. Accordingly, in the as-deposited DC Co–P 1 coating, $Co2p_{3/2,1/2}$ peaks at 778.1 and 793.1 eV with spin-orbit separation of 15 eV correspond to Co metal, whereas peaks at 781.8 and 797.6 eV with 15.8 eV spin-orbit separation is attributed to Co^{2+} from highly ionic Co^{2+} type of species present in this kind of coatings.[34–36] This highly ionic Co species corresponds to $Co(OH)_2$. There is an increase in Co metal concentration with increase in P amount. Mostly, oxidized Co along with metallic species is

present in as-deposited Co coating. However, concentration of oxidized Co increases in the alloys after corrosion in lower P content coating and there is no significant change in metallic as well as oxidized Co in the coating with higher P. Oxidized Co species is more in Co coating after corrosion. On other hand, mainly oxidized Co species is obtained in as-deposited PC Co and Co–P coatings that is contrary to DC deposited coatings. PC Co–P 1 coating shows the presence of small amount of Co metal, but PC Co–P 2 and PC Co–P 3 coatings contain Co^{2+} species only. It is interesting to note that Co metal concentration increases in PC Co–P 3 coating after corrosion. Co is in fully oxidized state in PC Co coating after corrosion. Representatively, binding energies, relative intensities and FWHMs of different Co species as obtained from Co2p spectra of as-deposited and corroded DC and PC Co–P 1 and Co–P 3 coatings are summarized in Tables 4 and 5, respectively.

XPS of P2p core level in as-deposited as well as corroded DC and PC Co–P coatings were also recorded. Typical core level P2p of as-deposited and corroded DC Co–P coatings are given in Fig. 11. P2p peak is considered as a single peak due to very small binding energy difference (0.9 eV) between $P2p_{3/2}$ and $P2p_{1/2}$ core levels. XPS of P2p in as-deposited DC Co–P 1 alloy shows two peaks at 129.9 and 133.8 eV. P2p core level binding energy in red phosphorous is observed to be at 130.65 eV.[37] Therefore, P2p peak in the DC Co–P 1 alloy coating is shifted by –0.75 eV in the lower binding energy side in relation to red phosphorous indicating that P is in a negatively charged state ($P^{\delta-}$) which corresponds to P of bulk Co–P alloy coating. Thus, a weak charge transfer from Co to P takes place in Co−P alloy and as P accepts electrons, P species interacting with Co in the alloy coating is negatively charged. Similar type of negative shifts has been observed in Cr−P, Mn−P and Ni−P alloys.[38−40] Helfand et al. have also noticed similar phenomenon in their study for Co–P coatings with high P content in acidic

medium.[20] It is seen that this type of charge transfer can also be observed in neutral medium like NaCl studied here. However, DC Co–P 3 coating shows two higher binding energy peaks at 131.2 and 133.4 eV that are attributed to oxidized P species in +1 (P^{+}) and +5 (P^{5+}) oxidation states, respectively.[20,39–42] Presence of both bulk and oxidized P species in the as-deposited DC Co−P coatings agrees well with the literature.[43] DC Co–P 1 contains P^{+} and P^{5+} species, whereas $P^{\delta-}$, P^{+} and P^{5+} species are present in the DC Co–P 2 and DC Co–P 3 coatings after corrosion. On the other hand, $P^{\delta-}$ and P^{5+} species are present in as-deposited PC coatings and after corrosion all coatings contain $P^{\delta-}$, P^{+} and P^{5+} species. However, PC Co–P 1 coating contains mainly oxidized species, whereas bulk P is major species in PC Co–P 2 and PC Co–P 3 coatings. Representatively, binding energies, relative intensities and FWHMs of different P species as obtained from P2p spectra of as-deposited and corroded DC and PC Co–P 1 and Co–P 3 coatings are summarized in Tables 6 and 7, respectively.

The spectral features of XPS of O1s core level region of as-deposited and corroded Co–P alloy coatings were also investigated. In all cases, spectra are observed to be broad and are resolved into several component peaks. Typical core level O1s spectra of as-deposited and corroded PC Co–P 3 coating are shown in Fig. 12. Peaks around 530.6 and 533.7 eV in as-deposited and corroded coatings correspond to O^{2-} type of species associated with Co^{2+} ion and adsorbed H_2O species, respectively.[19,44] On the other hand, an intense peak located around 532.0 eV is assigned for oxygen associated with P^{5+}. Most probable P related species for this higher binding energy peak is phosphate (PO_4^{3-}).[39,41,45] Again, alkalization of the electrolyte occurs at the cathode layer due to hydrogen evolution during electrodeposition leading to the formation of $Co(OH)_2$ species on the Co–W alloy coating surface which is evident from Co2p core level spectrum of as-deposited coating.[35] O1s binding energy value of oxygen attached with P is close

to that of metal hydroxide species with little higher region.[19,41,43] So, its binding energy can overlap with that of metal hydroxide species. Therefore, formation of both $Co_3(PO_4)_2$ and $Co(OH)_2$ species can be possible on the as-deposited coating surface that augers well with the literature.[45] There is no significant change in the intensity of all component peaks after corrosion as can be seen in Fig. 12 (b).

XPS results demonstrate that the DC plated coating contains higher amount of Co metal while the PC plated coatings contain more of Co oxide species. Corrosion experiments show that the PC coatings resist corrosion better than the DC coatings. This is due to the lower concentration of metal in PC coatings in which active dissolution of metals is suppressed due to the presence of metal oxide species. Basically, dissolution of metals in a corrosive medium is oxidation. Formation of oxide species after corrosion shows that the metallic cobalt species has undergone oxidation during dissolution. EDXS reveals that after corrosion there is a significant increase in the P content for both DC and PC deposited coatings with low P content, whereas only a marginal increase is observed in high P content coatings (Table 3). This implies that uniform corrosion would have occurred in the NaCl medium and enriched P layer over the surface and higher metal oxide content has inhibited further dissolution of cobalt and increases the corrosion resistance especially for PC plated coatings. Again, PC coatings are less affected by corrosion in relation to DC coatings as evident from FESEM studies. Therefore, PC deposition produces high quality Co–P coatings that contain smooth and compact morphology. Especially, there is no significant change in morphology of PC Co–P 3 coating after corrosion that leads to show lowest Q_{dl} value as obtained from EIS data indicating its superiority regarding corrosion resistance. As XPS studies demonstrate that Co is in fully oxidized state in PC Co–P 3 coating, possibility of inhibition of further dissolution of cobalt is much more than other

coatings. Hence, PC Co–P 3 coating shows best corrosion resistance property among all the coatings studied in the present work.

4. Conclusions

Co–P coatings with varying P contents were electrodeposited from chloride based bath employing direct and pulse current electrodeposition methods and their corrosion behavior was evaluated in details. Compositional analysis shows increasing amount of phosphorous has been incorporated into the coatings as the concentration of NaH_2PO_2 increases in the bath in both DC and PC electrodeposited coatings. A significant increase of P content has been observed on the surface of the low P coatings after corrosion showing active dissolution of these coatings in the corrosion medium, whereas high P coatings show only a marginal increase in P after corrosion exhibiting better corrosion resistance. XRD studies reveal that the low P coatings obtained by DC and PC methods are crystalline (fcc phase) which are transformed to amorphous (via hcp phase) with increasing P content. Electrochemical corrosion tests demonstrate that DC Co–P 3 and PC Co–P 3 coatings show lower corrosion current density (i_{corr}) and higher polarization resistance (R_p) while the PC plated coatings withstand corrosion better than their DC counterparts owing to their smooth and compact morphologies though these coatings are amorphous in nature. XPS studies exhibit the presence of oxide species of cobalt in PC coatings while DC plated coatings mainly consist of metallic Co. Higher corrosion resistance of PC plated coatings has also been attributed to the presence of higher amount of cobalt oxide species in these coatings. For high P coatings, though DC Co–P 3 and PC Co–P 3 seems to behave in a similar manner, pulse deposited high phosphorous coating (PC Co–P 3) shows very good corrosion resistance due to its amorphous structure, smooth and compact morphology and presence of higher amount of oxidized Co species in the as-deposited condition.

Acknowledgments

Authors would like to thank the Director, CSIR–National Aerospace Laboratories for giving permission to publish this work. Authors wish to acknowledge the help rendered by Mr. Siju for carrying out FESEM. Authors are thankful to Prof. M. S. Hegde, Indian Institute of Science, Bangalore for providing XPS facility.

References

1 I. Costa, N. Imaz, N. Cinca, E. Gorcía-Lecina, M. Sarret and C. Müller, *Trans. Inst. Met. Finish.*, 2012, **90**, 252.

2 R. A. Prado, F. Facchini, N. Mahalanobis, F. Gonzalez, G. Palumbo, Department of Defense (DoD) Corrosion Conference, Washington DC, 10th–14th August, 2009.

3 P. Choi, M. da Silva, U. Klement, T. Al-Kassab and R. Kirchheim, *Acta Mater.*, 2005, **53**, 4473.

4 M. da Silva, C. Wille, U. Klement, P. Choi and T. Al-Kassab, *Mater. Sci. Eng. A*, 2007, **445–446**, 31.

5 Y. Fukunaka, S. Aikawa and Z. Asaki, *J. Electrochem. Soc.*, 1994, **141**, 1783.

6 S. S. Djokić, *J. Electrochem. Soc.*, 1999, **146**, 1824.

7 V. Ezhilselvi, H. Seenivasan and K. S. Rajam, *Surf. Coat. Technol.*, 2012, **206**, 2199.

8 I. Kosta, A. Vicenzo, C. Müller and M. Sarret, *Surf. Coat. Technol.*, 2012, **207**, 443.

9 P. Bera, H. Seenivasan, K. S. Rajam and V. K. W. Grips, *Appl. Surf. Sci.*, 2012, **258**, 9544.

10 H. Seenivasan, P. Bera, K. S. Rajam and S. K. Parida, *Surf. Rev. Lett.*, 2013, **20**, 1350049.

11 N. R. Nik Masdek and A. Alfantazi, *ECS Trans.*, 2010, **28**, 249.

12 I. Kosta , E. Vallés, E. Gómez, M. Sarret and C. Müller, *Mater. Lett.*, 2011, **65**, 2849.

13 M. A. Sheikholeslam, M. H. Enayati and K. Raeissi, *Mater. Lett.*, 2008, **62**, 3629.

14 F. Cebollada, J. M. González, C. de Julian and S. Suriñach, *Phys. Rev. B*, 1997, **56**, 6056.

15 X. Xu and G. Zangari, *J. Appl. Phys.*, 2006, **99**, 08M304.

16 B. Gillot, K. E1 Amri, P. Pouderoux, J. P. Bonino and A. Rousset, *J. Alloys Compd.*, 1992, **189**, 151.

17 A. Aledresse and A. Alfantazi, *J. Mater. Sci.*, 2004, **39**, 1523.

18 H. Jung and A. Alfantazi, *Electrochim. Acta*, 2006, **51**, 1806.

19 H. Jung and A. Alfantazi, *Corrosion*, 2007, **63**, 159.

20 M. A. Helfand, C. R. Clayton, K. B. Diegle and N. R. Sorenson, *J. Electrochem. Soc.*, 1992, **139**, 2121.

21 M. A. Sheikholeslam, R. Raeissi and M. H. Enayati, *Trans. Inst. Met. Finish.*, 2010, **88**, 324.

22 B. A. Boukamp, *J. Electrochem. Soc.*, 1995, **142**, 1885.

23 M. Stern and A. L. Geary, *J. Electrochem. Soc.*, 1957, **104**, 56.

24 A. Vicenzo and P. L. Cavallotti, *Electrochim. Acta*, 2004, **49**, 4079.

25 S. Nakahara and S. Mahajan, *J. Electrochem. Soc.*, 1980, **127**, 283.

26 T. Cohen-Hyams, W. D. Kaplan and J. Yahalom, *Electrochem. Solid-State Lett.*, 2002, **5**, C75.

27 R. Sard, C. D. Schwartz and R. Weil, *J. Electrochem. Soc.*, 1966, **113**, 424.

28 L. Cadorna and P. Cavalloti, *Electrochim. Metallorum.*, 1966, **1**, 364.

29 J. R. Macdonald, *Impedance Spectroscopy: Emphasizing Solid Materials and Systems*, John Wiley & Sons, New York, 1987, p. 17.

30 X.-Z. Yuan, C. Song, H. Wang and J. Zhang, *Electrochemical Impedance Spectroscopy in PEM Fuel Cells, Fundamentals and Applications*, Springer, London, 2010, p. 140.

31 A. A. Karimpoor, K. T. Aust and U. Erb, *Script. Mater.*, 2007, **56**, 201.

32 J. A. Tesk, C. E. Johnson, D. Skrtic, M. Tung and S. Hsu, *Amorphous Alloys Containing Cobalt for Orthopaedic Applications*, in Cobalt-Base Alloys for Biomedical Applications, ASTM STP 1365, eds., J. A. Disegi, R. L. Kennedy and R. Pilliar, Eds., American Society for Testing and Materials, West Conshohocken, 1999.

33 J.-C. Puippe and F. Leaman, *Theory and Practice of Pulse Plating*, American Electroplaters and Surface Finishers Society, Orlando, 1986.

34 N. S. Mclntyre and M. G. Cook, *Anal. Chem.*, 1975, **47**, 2208.

35 L. Orlovskaja, E. Matulionis, A. Timinskas and V. Šukienė, *Surf. Coat. Technol.*, 2000, **135**, 34.

36 C. N. R. Rao, D. D. Sarma, S. Vasudevan and M. S. Hegde, *Proc. R. Soc. Lond. A*, 1979, **367**, 239.

37 R. Franke, T. Chassé, P. Streubel and A. Meisel, *J. Electron Spectrosc. Relat. Phenom.*, 1991, **56**, 381.

38 M. Pelavin, D. N. Hendrickson, J. M. Hollander and W. L. Jolly, *J. Phys. Chem.*, 1970, **74**, 1116.

39 K. S. Rajam, S. R. Rajagopalan, M. S. Hegde and B. Viswanathan, *Mater. Chem. Phys.*, 1991, **27**, 141.

40 B. Elsener, M. Crobu, M. A. Scorciapino and A. Rossi, *J. Appl. Electrochem.*, 2008, **38**, 1053.

41 C. L. Aravinda, P. Bera, V. Jayaram and S. M. Mayanna, *Appl. Surf. Sci.*, 2002, **191**, 128.

42 D. Barreca, A. Camporese, M. Casarin, N. El Habra, A. Gasparotto, M. Natali, G. Rossetto, E. Tondello and P. Zanella, *J. Electrochem. Soc.*, 2004, **151**, G638.

43 K. Shimizu, K. Kobayashi, P. Skeldon, G. E. Thompson, G. C. Wood, *Mater. Sci. Eng.* A, 1995, **198**, 35.

44 P. Bera, H. Seenivasan and K. S. Rajam, *Surf. Rev. Lett.*, 2013, **20**, 1350006.

45 T. Chassé, R. Franke, C. Urban, R. Franzheld, P. Streubel and A. Meisel, *J. Electron Spectrosc. Relat. Phenom.*, 1993, **62**, 287.

Table 1. Potentiodynamic polarization data of DC and PC deposited Co and Co–P coatings.

Coatings	E_{corr} (V)	i_{corr} ($\mu A\ cm^{-2}$)	R_p ($k\Omega\ cm^2$)
DC Co	–0.613	3.2	7.1
DC Co–P 1	–0.497	2.7	8.4
DC Co–P 2	–0.430	2.0	12.0
DC Co–P 3	–0.480	0.8	22.6
PC Co	–0.536	3.0	10.4
PC Co–P 1	–0.386	1.0	20.2
PC Co–P 2	–0.397	0.8	21.0
PC Co–P 3	–0.411	0.5	25.6

Table 2. EIS data of DC and PC deposited Co and Co–P coatings.

Coatings	R_s (Ω cm^2)	Q_{dl}–Y_0 (μSs^n cm^{-2})	n_{dl}	R_{ct} ($k\Omega$ cm^2)
DC Co	10.2	17.0	0.79	3.2
DC Co–P 1	10.0	12.7	0.80	5.0
DC Co–P 2	10.7	13.7	0.91	9.1
DC Co–P 3	12.5	25.7	0.88	13.6
PC Co	9.5	13.6	0.80	5.8
PC Co–P 1	9.7	35.6	0.91	23.8
PC Co–P 2	8.5	39.7	0.92	22.4
PC Co–P 3	11.0	5.8	0.94	45.8

Table 3. Concentration (wt.%) of P in as-deposited and after corrosion DC and PC Co–P coatings evaluated from EDXS.

Coatings	As-deposited	After corrosion
DC Co–P 1	3.7	6
DC Co–P 2	8	8
DC Co–P 3	9.4	10
PC Co–P 1	2.5	7
PC Co–P 2	8.6	9
PC Co–P 3	11.2	10

Table 4. Binding energies, relative intensities and FWHMs of different Co species as observed from Co2p of before and after corrosion DC Co–P coatings.

Coatings	DC Co–P 1			DC Co–P 3		
	Co species	Binding energy of $Co2p_{3/2}$ (eV)	Relative intensity (%)	Co species	Binding energy of $Co2p_{3/2}$ (eV)	Relative intensity (%)
As-deposited	Co^0 Co^{2+}	778.1 781.8	40 60	Co^0 Co^{2+}	778.2 781.3	62 38
After corrosion	Co^{2+}	781.7	100	Co^0 Co^{2+}	778.1 781.5	61 39

Table 5. Binding energies, relative intensities and FWHMs of different Co species as observed from Co2p of before and after corrosion PC Co–P coatings.

Coatings	PC Co–P 1			PC Co–P 3		
	Co species	Binding energy of $Co2p_{3/2}$ (eV)	Relative intensity (%)	Co species	Binding energy of $Co2p_{3/2}$ (eV)	Relative intensity (%)
As-deposited	Co^0 Co^{2+}	777.9 781.7	28 72	Co^{2+}	781.8	100
After corrosion	Co^{2+}	781.8	100	Co^0 Co^{2+}	778.1 783.0	41 59

Table 6. Binding energies, relative intensities and FWHMs of different P species as observed from P2p of before and after corrosion DC Co–P coatings.

Coatings	DC Co–P 1			DC Co–P 3		
	P species	Binding energy of P2p (eV)	Relative intensity (%)	P species	Binding energy of P2p (eV)	Relative intensity (%)
As-deposited	$P^{\delta-}$	129.9	22	$P^{\delta-}$	129.8	68
	P^{5+}	133.8	78	P^{+}	131.2	19
				P^{5+}	133.4	13
After corrosion	P^{+}	131.2	40	$P^{\delta-}$	129.9	64
	P^{5+}	133.5	60	P^{+}	131.5	18
				P^{5+}	133.7	18

Table 7. Binding energies, relative intensities and FWHMs of different P species as observed from P2p of before and after corrosion PC Co–P coatings.

Coatings	PC Co–P 1			PC Co–P 3		
	P species	Binding energy of P2p (eV)	Relative intensity (%)	P species	Binding energy of P2p (eV)	Relative intensity (%)
As-deposited	$P^{\delta-}$	129.7	32	$P^{\delta-}$	130.0	58
	P^{5+}	133.2	68	P^{5+}	133.5	42
After corrosion	$P^{\delta-}$	130.0	09	$P^{\delta-}$	130.0	70
	P^{5+}	134.1	60	P^{+}	131.6	10
	P^{6+}	136.4	31	P^{5+}	133.3	20

Figure captions

Fig. 1 XRD patterns of as-deposited DC and PC Co–P coatings.

Fig. 2 Potentiodynamic polarization curves obtained for DC and PC Co–P coatings.

Fig. 3 (a) Nyquist plots and (b) Bode plots of Co–P coatings deposited by DC plating: (●) MS, (♦) DC Co, (*) DC Co–P 1 (▼) DC Co–P 2 and (▲) DC Co–P 3.

Fig. 4 (a) Nyquist plots and (b) Bode plots of Co–P coatings deposited by PC plating: (●) MS, (♦) PC Co, (*) PC Co–P 1 (▼) PC Co–P 2 and (▲) PC Co–P 3.

Fig. 5 Equivalent circuit used for fitting the electrochemical data of DC and PC deposited coatings.

Fig. 6 FESEM images of as-deposited Co–P coatings prepared by DC plating method: (a) DC Co (b) DC Co–P 1, (c) DC Co–P 2 and (d) DC Co–P 3.

Fig. 7 FESEM images of as-deposited Co–P coatings prepared by PC plating method: (a) PC Co, (b) PC Co–P 1, (c) PC Co–P 2 and (d) PC Co–P 3.

Fig. 8 FESEM images of corroded Co–P coatings prepared by DC plating method: (a) DC Co, (b) DC Co–P 1, (c) DC Co–P 2 and (d) DC Co–P 3.

Figure 9. FESEM images of corroded Co–P coatings prepared by PC plating method: (a) PC Co, (b) PC Co–P 1, (c) PC Co–P 2 and (d) PC Co–P 3.

Fig. 10 XPS of Co2p core levels in (a) as-deposited DC, (b) corroded DC, (c) as-deposited PC and (d) corroded PC Co–P coatings.

Fig. 11 XPS of P2p core levels in (a) as-deposited DC, (b) corroded DC, as-deposited PC and (d) corroded Co–P coatings.

Fig. 12 XPS of O1s core levels in (a) as-deposited and (b) corroded PC Co–P 3 coatings.

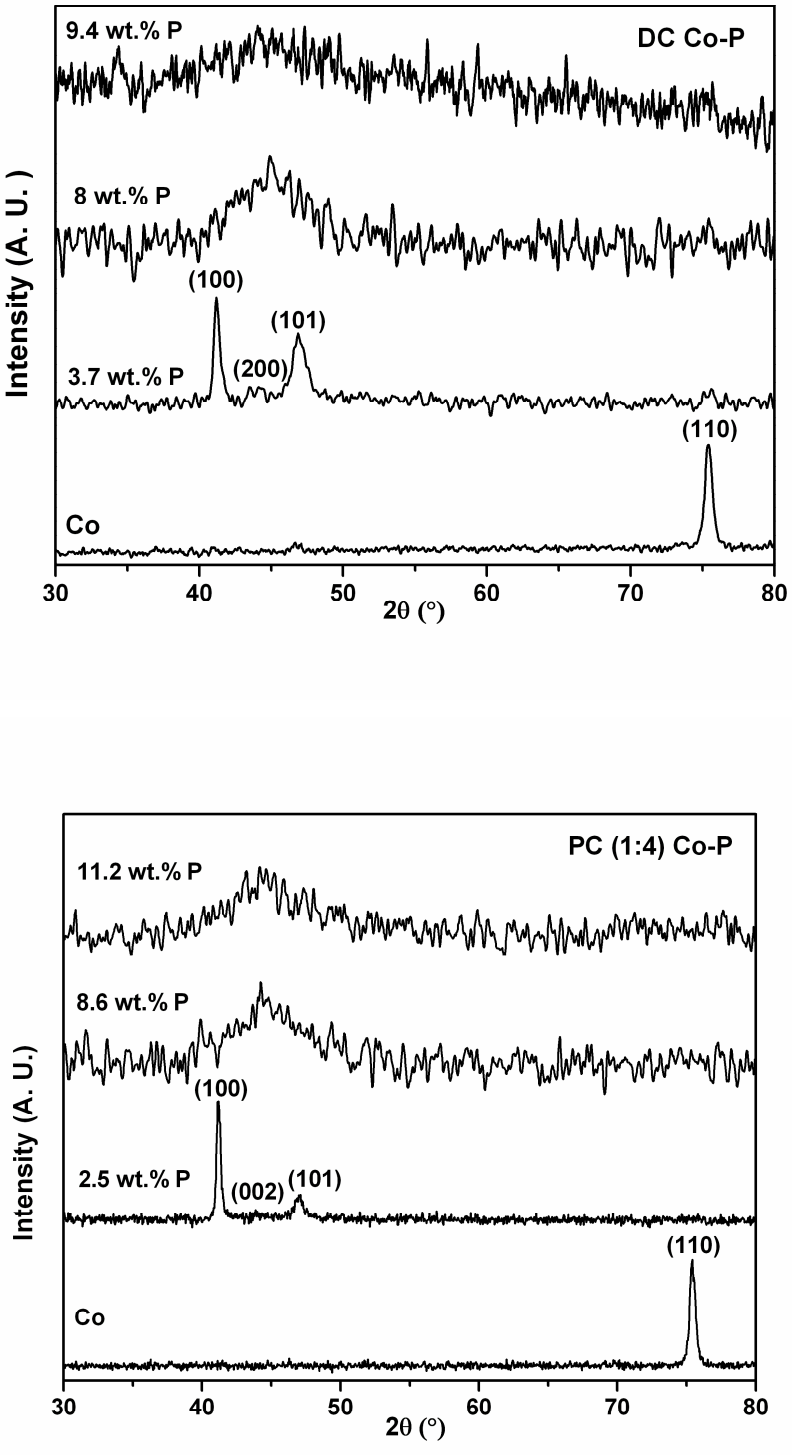

Fig. 1 XRD patterns of as-deposited DC and PC Co–P coatings.

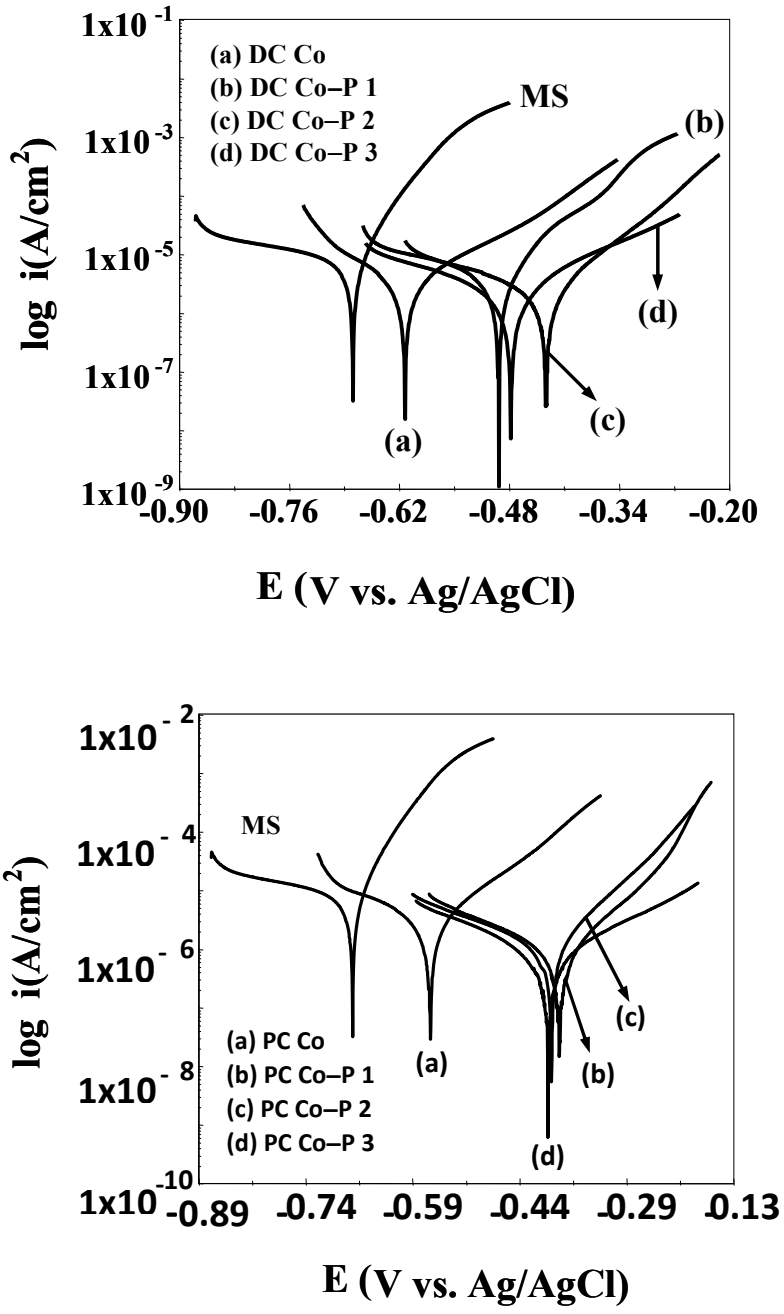

Fig. 2 Potentiodynamic polarization curves obtained for DC and PC Co–P coatings.

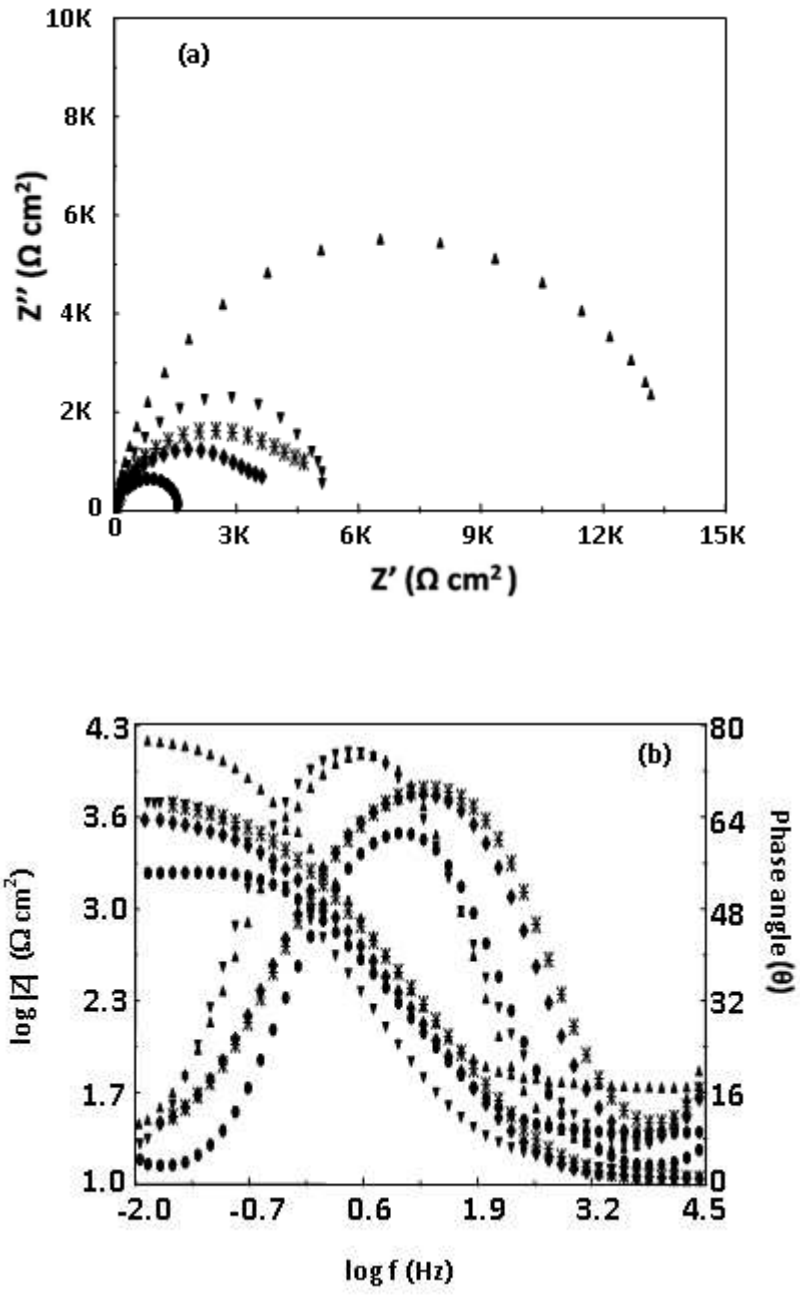

Fig. 3 (a) Nyquist plots and (b) Bode plots of Co–P coatings deposited by DC plating: (●) MS, (♦) DC Co, (*) DC Co–P 1 (▼) DC Co–P 2 and (▲) DC Co–P 3.

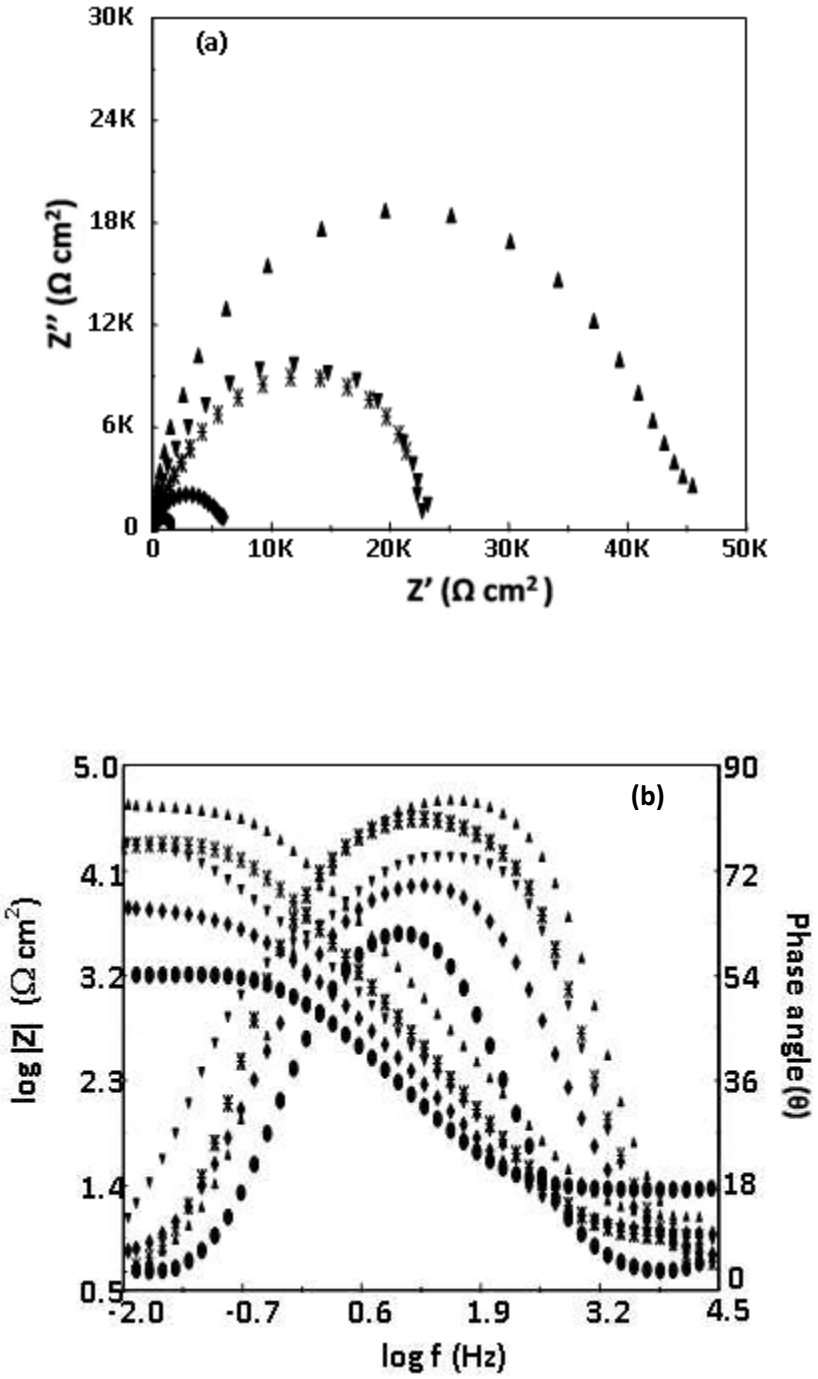

Fig. 4 (a) Nyquist plots and (b) Bode plots of Co–P coatings deposited by PC plating: (●) MS, (♦) PC Co, (*) PC Co–P 1 (▼) PC Co–P 2 and (▲) PC Co–P 3.

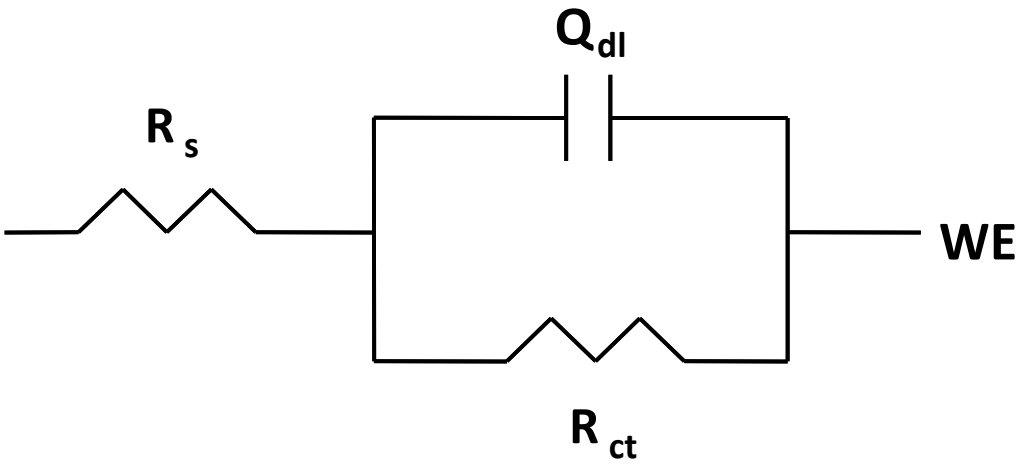

Fig. 5 Equivalent circuit used for fitting the electrochemical data of DC and PC deposited coatings.

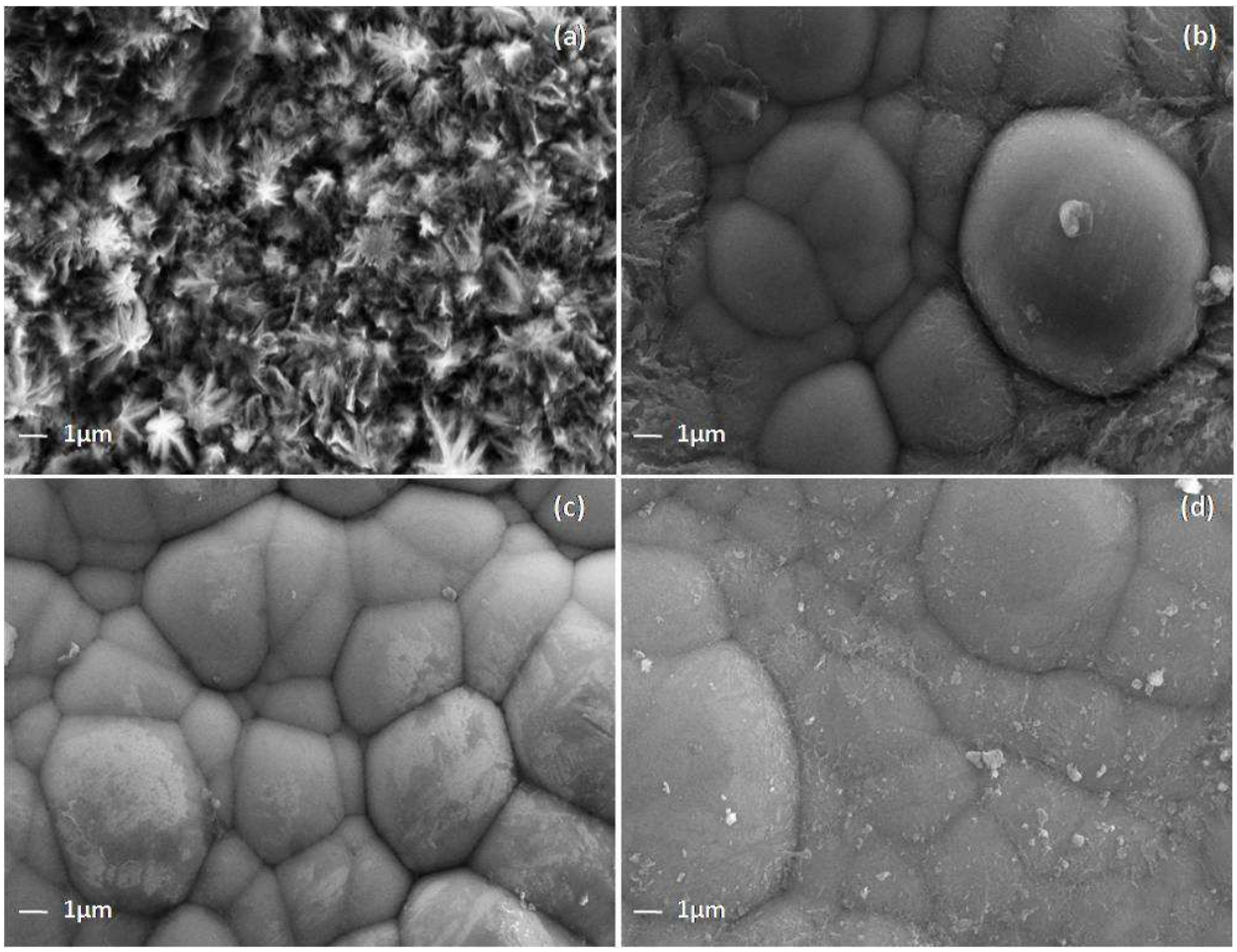

Fig. 6 FESEM images of as-deposited Co–P coatings prepared by DC plating method: (a) DC Co (b) DC Co–P 1, (c) DC Co–P 2 and (d) DC Co–P 3.

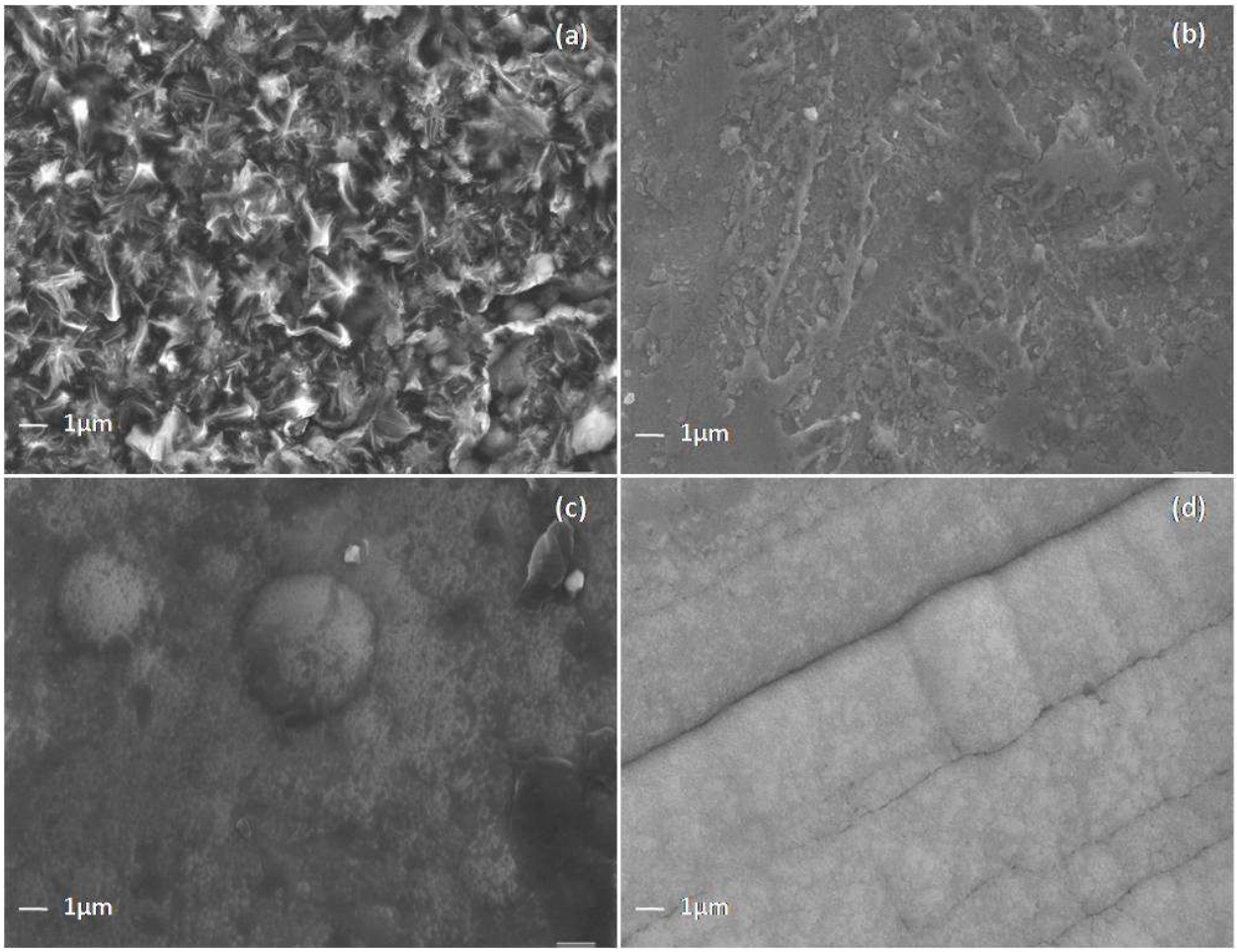

Fig. 7 FESEM images of as-deposited Co–P coatings prepared by PC plating method: (a) PC Co, (b) PC Co–P 1, (c) PC Co–P 2 and (d) PC Co–P 3.

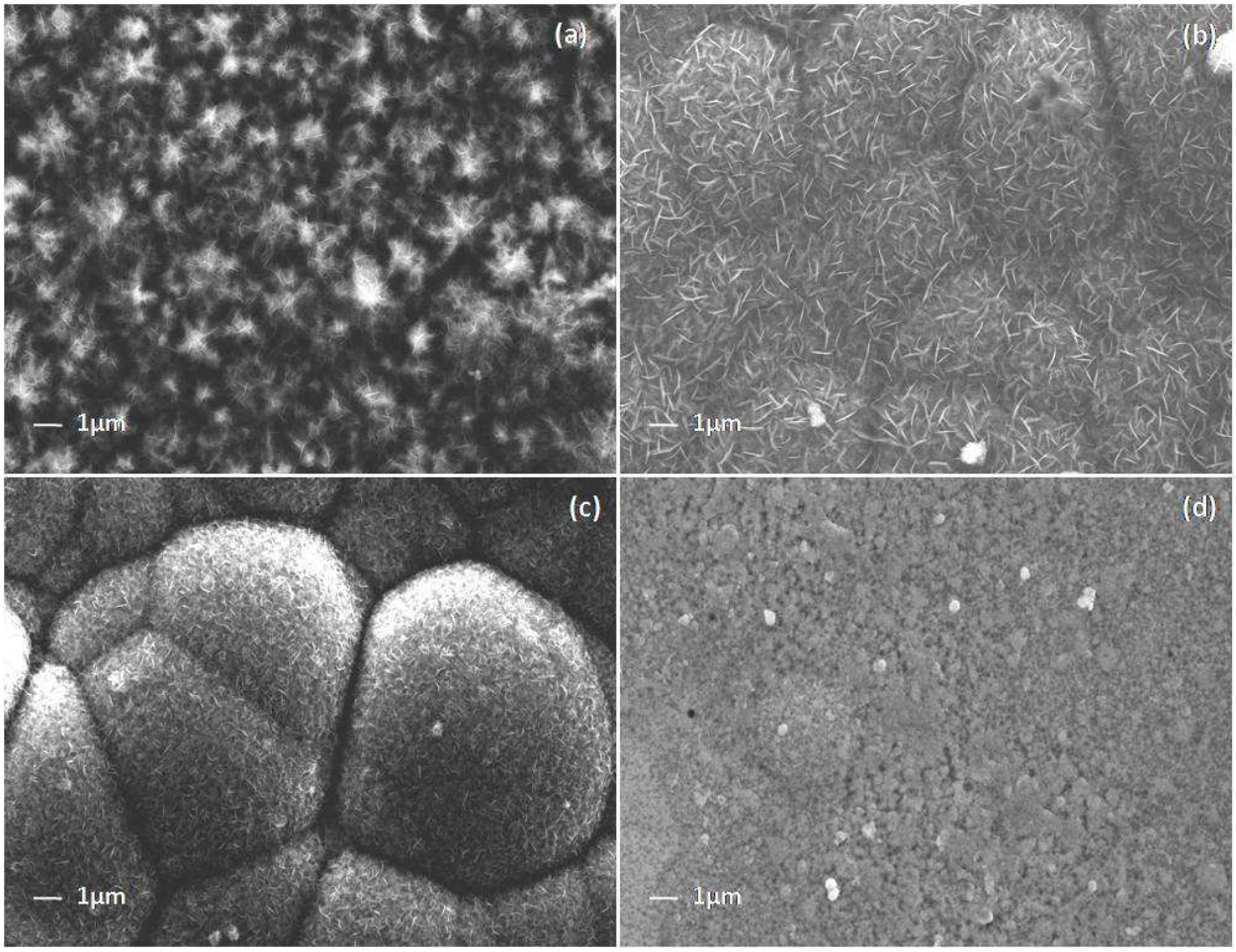

Fig. 8 FESEM images of corroded Co–P coatings prepared by DC plating method: (a) DC Co, (b) DC Co–P 1, (c) DC Co–P 2 and (d) DC Co–P 3.

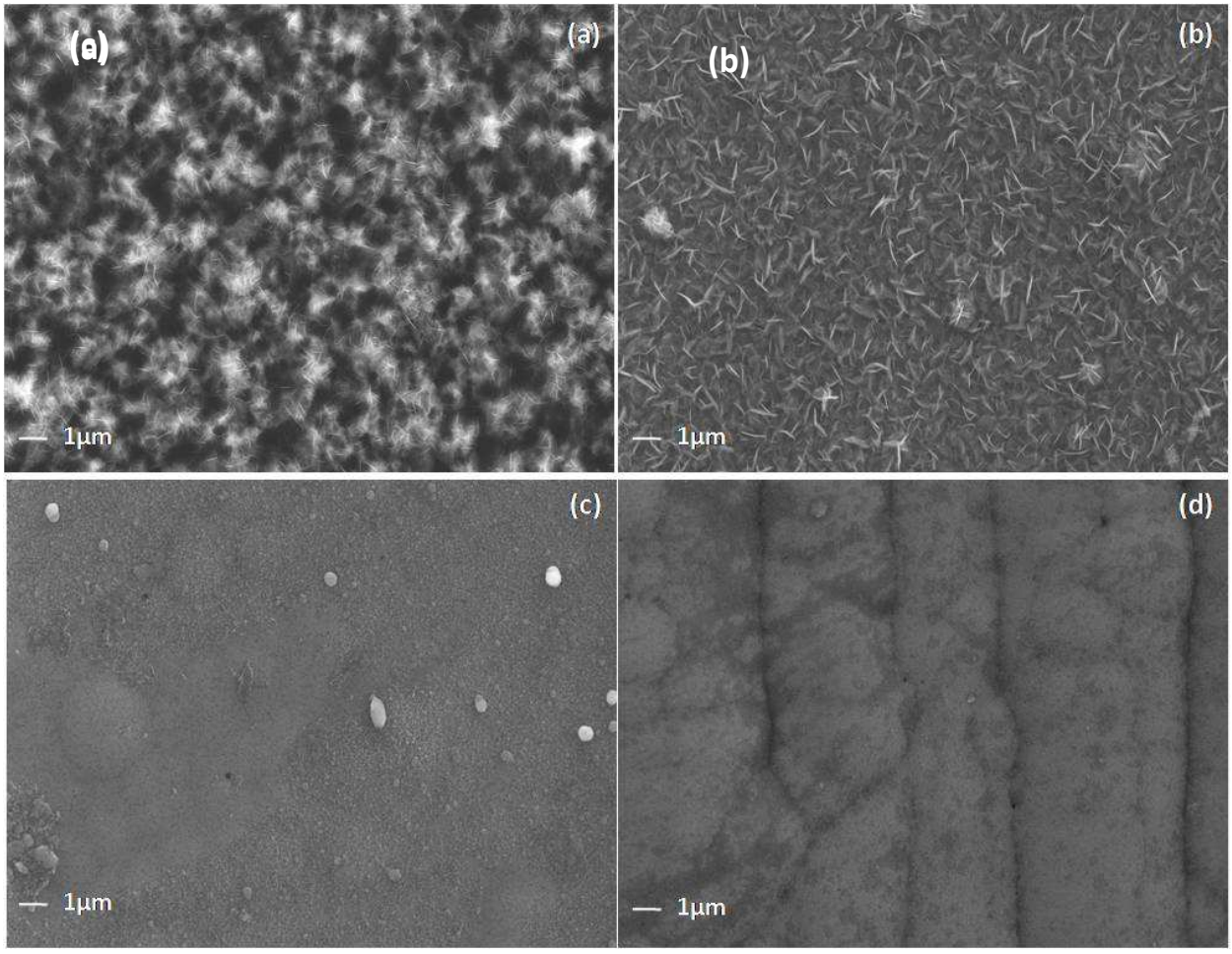

Fig. 9 FESEM images of corroded Co–P coatings prepared by PC plating method: (a) PC Co, (b) PC Co–P 1, (c) PC Co–P 2 and (d) PC Co–P 3.

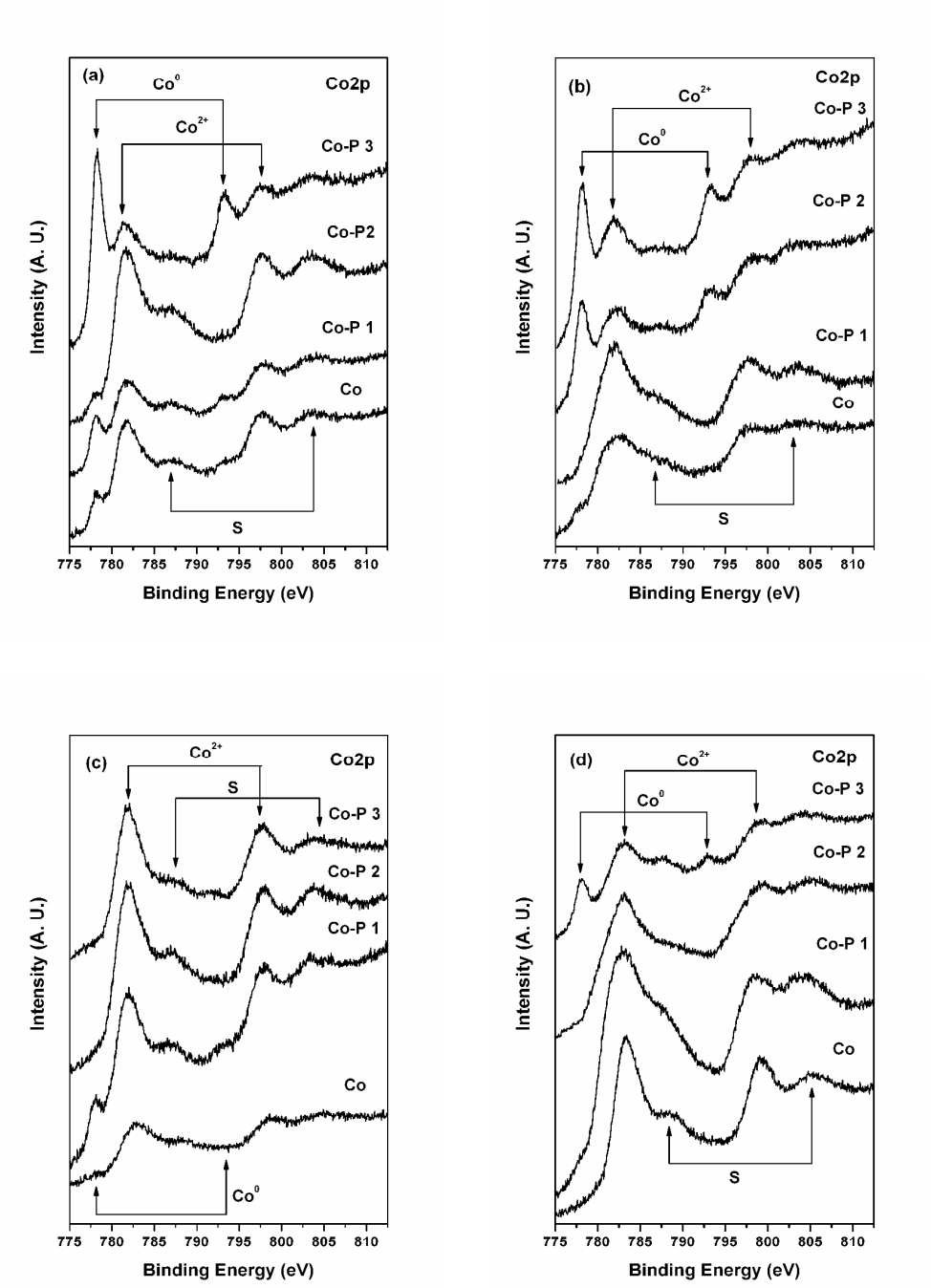

Fig. 10 XPS of Co2p core levels in (a) as-deposited DC, (b) corroded DC, (c) as-deposited PC and (d) corroded PC Co–P coatings.

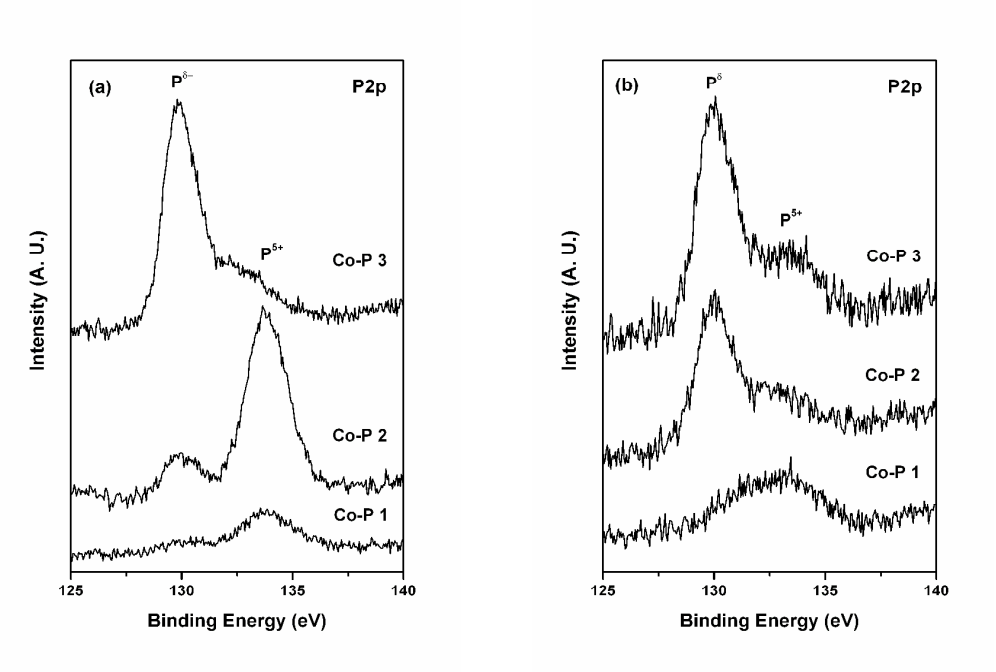

Fig. 11 XPS of P2p core levels in (a) as-deposited and (b) corroded DC Co–P coatings.

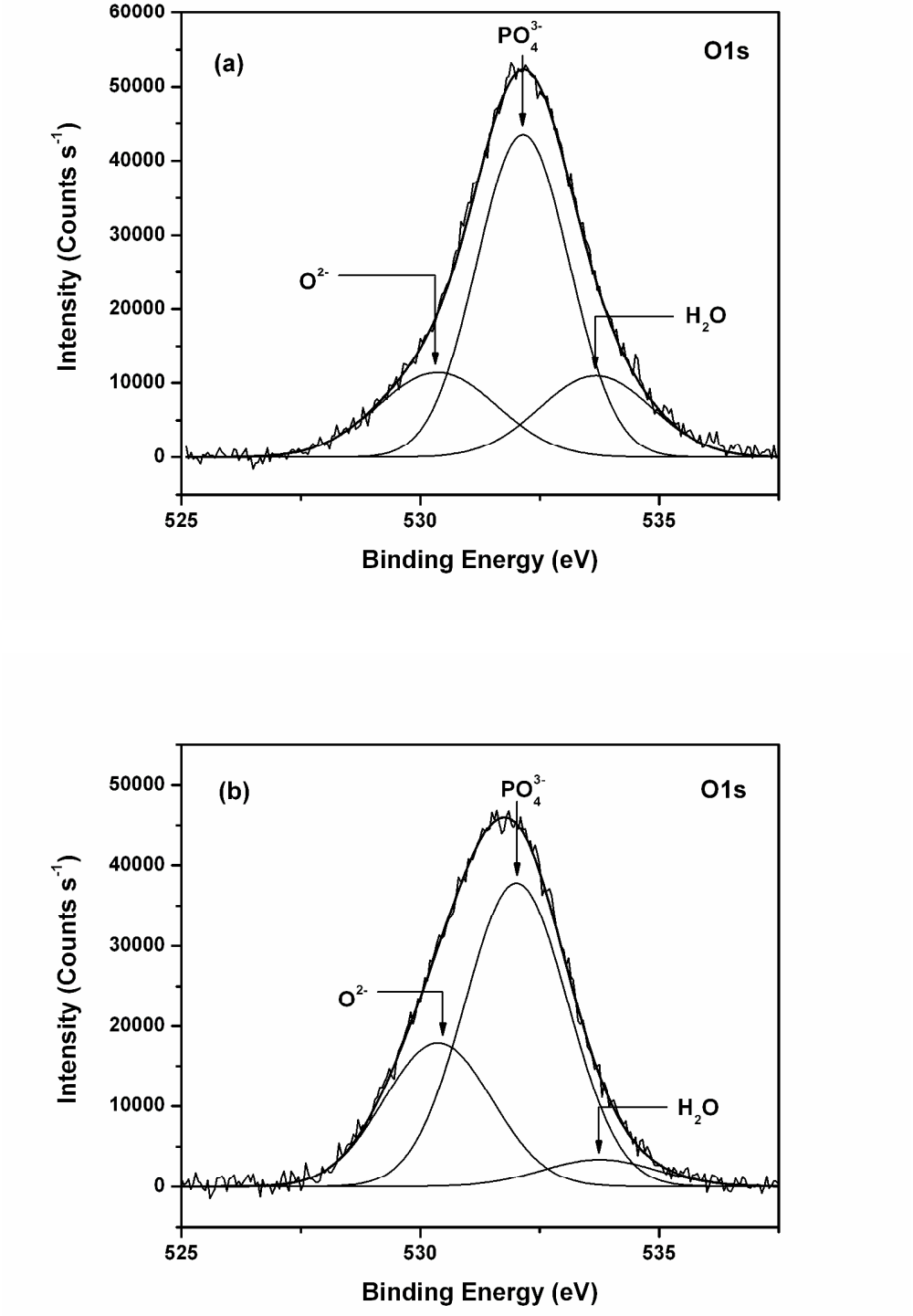

Fig. 12 XPS of O1s core levels in (a) as-deposited and (b) corroded PC Co–P 3 coatings.